MICHIGAN STATE UNIVERSITY

CYCLOTRON LABORATORY

TWO-PROTON CORRELATION FUNCTIONS FOR EQUILIBRIUM AND NON-EQUILIBRIUM EMISSION

C.K. GELBKE; W.G. GONG; W. BAUER; N. CARLIN;
R.T. de SOUZA; Y.D. KIM; W.G. LYNCH;
T. MURAKAMI; G. POGGI; M.B. TSANG; H.M. XU;
S. PRATT; D.E. FIELDS; K. KWIATKOWSKI;
R. PLANETA; V.E. VIOLA, JR.; and
S.J. YENNELLO

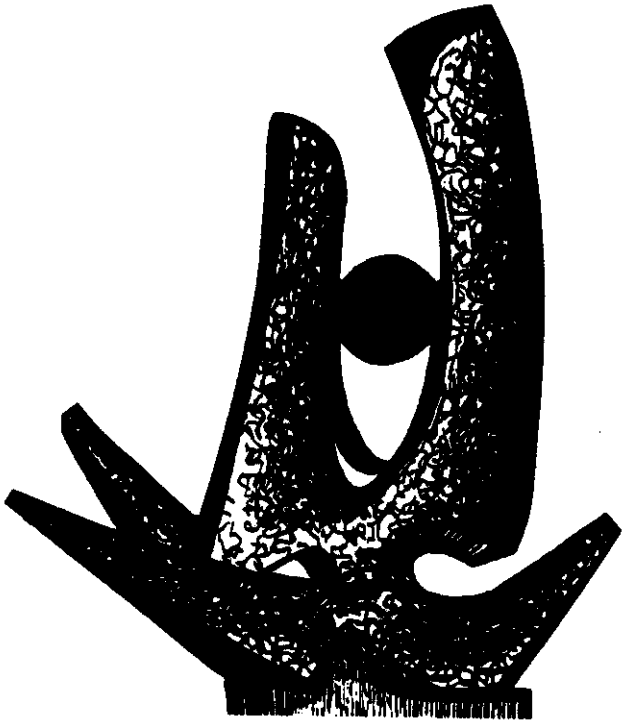

JULY 1990

MSUCL-732

MSUCL-732
July, 1990

"Two-proton correlation functions for equilibrium and non-equilibrium emission"

C.K. Gelbke, W.G. Gong, W. Bauer, N. Carlin*, R.T. de Souza, Y.D. Kim, W.G. Lynch, T. Murakami**, G. Poggi***, M.B. Tsang, and H.M. Xu
National Superconducting Cyclotron Laboratory and Department of Physics and Astronomy, Michigan State University, East Lansing, MI 48824, USA

S. Pratt
Department of Physics, University of Wisconsin, Madison, WI 53706, USA

D.E. Fields, K. Kwiatkowski, R. Planeta, V.E. Viola, Jr. and S.J. Yennello
Indiana University Cyclotron Facility, Indiana University, Bloomington, IN 47405, USA

1. ABSTRACT

Two-proton correlation functions are compared for equilibrium and non-equilibrium emission processes investigated, respectively, in "reverse kinematics" for the reactions $^{129}Xe+^{27}Al$ and $^{129}Xe+^{119}Sn$ at E/A-31 MeV and in "forward kinematics" for the reactions $^{14}N+^{27}Al$ and $^{14}N+^{197}Au$ at E/A=75 MeV. Observed differences in the shapes of the correlation functions are understood in terms of the different time scales for equilibrium and preequilibrium emission.

2. INTRODUCTION

Two protons, emitted at small relative momenta from an excited nuclear system, carry information about the space-time characteristics of the emitting source [1-11]. The shape of the two-proton correlation function reflects the interplay of the short-range attractive nuclear interaction, the Pauli exclusion principle, and the long range repulsive Coulomb interaction between the two emitted protons. The short range nuclear interaction is dominated by the attractive singlet S-wave nuclear interaction which leads to a pronounced maximum in the

a Present address: Instituto de Fisica, Universidade de São Paulo, C. Postal 20516, CEP 01498, São Paulo, Brazil
** Present address: Department of Physics, Kyoto University, Kyoto 606, Japan
*** Permanent address: Dlpartimento di Fisica dell' Universita and INFN, Largo Enrico Fermi 2, 50125 Firenze, Italy

two-proton correlation function at relative momentum q≈20 MeV/c, when the average distance upon emission is of the order of 10 fm or less [1]. The long range Coulomb interaction and the Pauli exclusion principle give rise to a minimum at q=0. Some directional information can be provided by antisymmetrization effects [1,7,8].

The average distance between two coincident protons upon emission depends on the spatial dimension, d, and the average lifetime, τ, of the emitting system; it is of the order of $d+\bar{v}\tau$, where $\bar{v}$ is the average velocity of the emitted protons. For the decay of equilibrated compound nuclei with temperatures below 5 MeV, estimated lifetimes are larger than several hundred fm/c [12]. As a consequence, the average distance between emitted particles is much larger than the size of the emitting nucleus and the effects of the Coulomb interaction and the Pauli principle should dominate. On the other hand, preequilibrium light particle emission in intermediate energy heavy ion collisions is calculated to proceed on much shorter time scales [13,14] and average particle separations may reflect the spatial dimension of the emitting system rather than the emission rate. Here, the nuclear interaction should be prominent.

We have performed a comparative study of two-proton correlation functions measured for preequilibrium and equilibrium emission processes. When light projectiles impinge on heavy target nuclei, preequilibrium emission is strongly enhanced at small angles, whereas equilibrium emission dominates at backward angles, see e.g. refs. [5,10,11]. Preequilibrium emission was studied in "forward kinematics" for the reactions $^{14}N+^{27}Al$ and $^{14}N+^{197}Au$ at E/A=75 MeV. Equilibrium emission was studied at a lower energy, E/A=31 MeV, in "reverse kinematics" for the reaction $^{129}Xe+^{27}Al$ and for the nearly symmetric system $^{129}Xe+^{122}Sn$.

3. EXPERIMENTAL DETAILS

The experiments were performed with beams from the K1200 cyclotron from the National Superconducting Cyclotron Laboratory at Michigan State University. For reactions induced by ^{129}Xe, we used ^{27}Al and

^{122}Sn targets with areal densities of 5.6 and 5.3 mg/cm^2, respectively. For reactions induced by ^{14}N, we used ^{27}Al and ^{197}Au targets with areal densities of 15.0 and 15.9 mg/cm^2, respectively. Light particles were detected with two ΔE-E detector arrays consisting of 300-400 μm thick silicon ΔE-detectors and 10 cm long CsI(Tl) or NaI(Tl) E-detectors. An array consisting of 37 Si-CsI(Tl) telescopes [15] was centered at the polar and azimuthal angles of θ=25° and ϕ=0°; each of its detectors had a solid angle of $\Delta\Omega$=0.37 msr and a nearest neighbor spacing of $\Delta\theta$=2.6°. Another array consisting of 13 Si-NaI(Tl) telescopes was centered at θ=25° and ϕ=90°; each of its detectors had a solid angle of $\Delta\Omega$=0.5 msr and a nearest neighbor spacing of $\Delta\theta$=4.4°. Coincidence and downscaled singles data were taken simultaneously. Energy calibrations are accurate to better than 2%. Typical detector energy resolutions were of the order of 2% and 1% for protons of 40 MeV and 100 MeV, respectively. All data were corrected for random coincidences.

4. BASIC EQUATIONS

The experimental two-particle correlation function, R(q), is defined in terms of the coincidence yield, $Y(\vec{p}_1,\vec{p}_2)$, and the single particle yields, $Y(\vec{p}_1)$ and $Y(\vec{p}_2)$:

$$\sum Y(\vec{p}_1,\vec{p}_2) = C\big(1+R(q)\big)\sum Y(\vec{p}_1)Y(\vec{p}_2) \ . \qquad (1)$$

Here, $\vec{p}_1$ and $\vec{p}_2$ are the laboratory momenta of particles 1 and 2, and q is the relative momentum of the particle pair. For each experimental gating condition, the sums on both sides of Eq. 1 are extended over all energy and detector combinations corresponding to the given bins of q. The normalization constant, C, is determined by the requirement that R(q)=0 for large relative momenta.

Our theoretical analysis is based on the expression [7,8]:

$$1+R(\vec{P},\vec{q}) = \int d^3r F_{\vec{P}}(\vec{r})\,|\phi(\vec{q},\vec{r})|^2 \ , \qquad (2)$$

where $\phi(\vec{q},\vec{r})$ is the relative two-proton wavefunction and $F_{\vec{P}}(\vec{r})$ is

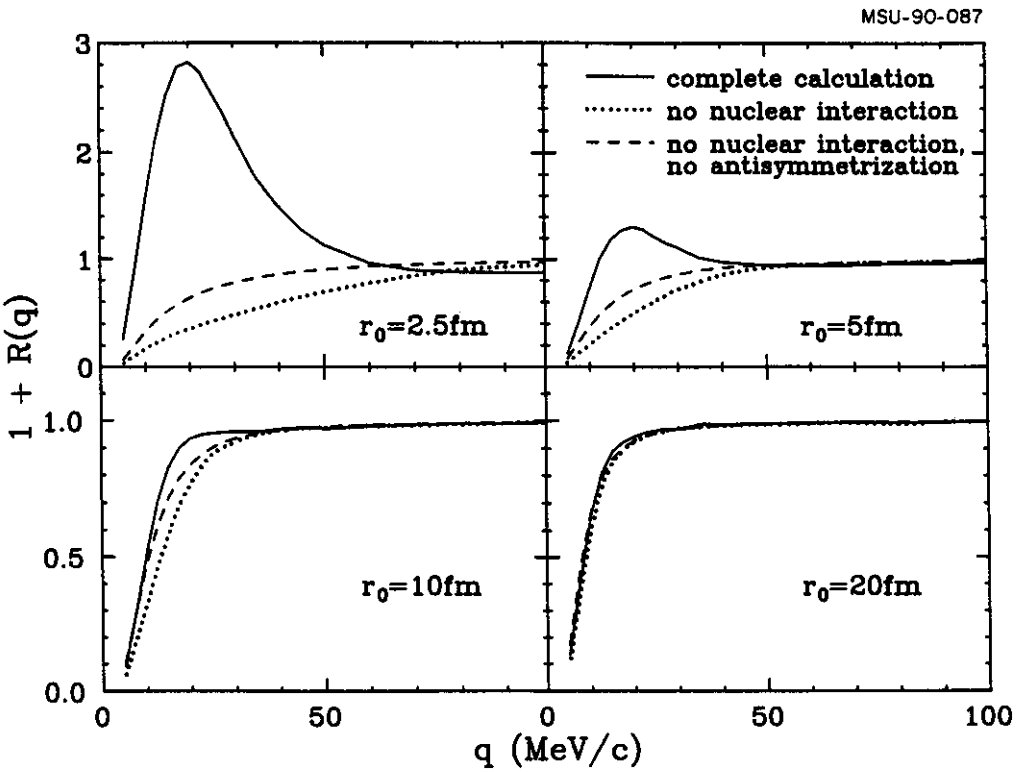

Fig. 1. Two-proton correlation functions calculated for short-lived Gaussian sources of representative radius parameters, r_0=2.5, 5, 10, 20 fm. The solid curves show the result of the full calculations; the dotted curves show calculations for which the nuclear interaction is neglected; the dashed curves shown calculations for which the nuclear interaction and the Pauli principle are neglected.

calculated correlation functions. For much larger source dimensions, $r_0 \gtrsim 20$ fm, the Coulomb interaction dominates and the Pauli principle can be neglected.

5. ANGLE AND ENERGY INTEGRATED CORRELATION FUNCTIONS

Two-proton correlation functions corresponding to sums over all detectors and all proton energies above the applied software threshold of 10 MeV are compared in Fig. 2. The correlation functions measured for the ^{14}N-induced reactions exhibit a minimum at q=0 MeV/c and a pronounced maximum at q≈20 MeV, see top panels of Fig. 2. In contrast, the correlation functions measured for the ^{129}Xe-induced reactions exhibit only a minimum at q≈0 MeV/c, see bottom panels of Fig. 2. For

defined by:

$$F_{\vec{p}}(\vec{r}) = \frac{\int d^3R f(\vec{P}/2,\vec{R}+\vec{r}/2,t_>) f(\vec{P}/2,\vec{R}-\vec{r}/2,t_>)}{|\int d^3r f(\vec{P}/2,\vec{r},t_>)|^2} . \qquad (3)$$

The Wigner function $f(\vec{p},\vec{x},t_>)$ is the phase-space distribution of particles of momentum $\vec{p}$ at position $\vec{x}$ at some time, $t_>$, after the emission process:

$$f(\vec{p},\vec{r},t_>) = \int_{-\infty}^{t_>} dt\, g(\vec{p},\vec{r}-\vec{v}_{\vec{p}}(t_>-t),t) . \qquad (4)$$

Here, $g(\vec{p},\vec{r},t)$ denotes the probability of emitting a particle with momentum $\vec{p}$ from location $\vec{r}$ and at time t.

The relative importance of antisymmtrization and the nuclear and Coulomb interactions depends on the size of the emitting system. In order to provide a quantitative comparison of these effects, we have calculated two-proton correlation functions for Gaussian sources of negligible lifetime,

$$g(\vec{p},\vec{r},t) = \rho_0 \exp(-r^2/r_0^2)\delta(t-t_0) \qquad (5)$$

in which the nuclear interaction and the Pauli principle were turned off successively. These calculations are compared in Fig. 1 for a number of representative radius parameters (r_0=2.5, 5, 10, 20 fm) . The solid curves show the results of the full calculations which include the nuclear and Coulomb interactions and the Pauli exclusion principle. The dotted lines show calculations for which the nuclear interaction has been turned off; these calculations still include the two-proton Coulomb interaction and the antisymmetrization of the relative wave function. The dashed curves represent calculations for which both the nuclear interaction and the antisymmetrization of the relative wave function have been turned off. For radius parameters, $r_0 \lesssim 10$ fm, both the antisymmetrization of the relative wave function and the nuclear interaction have important effects on the detailed shape of the

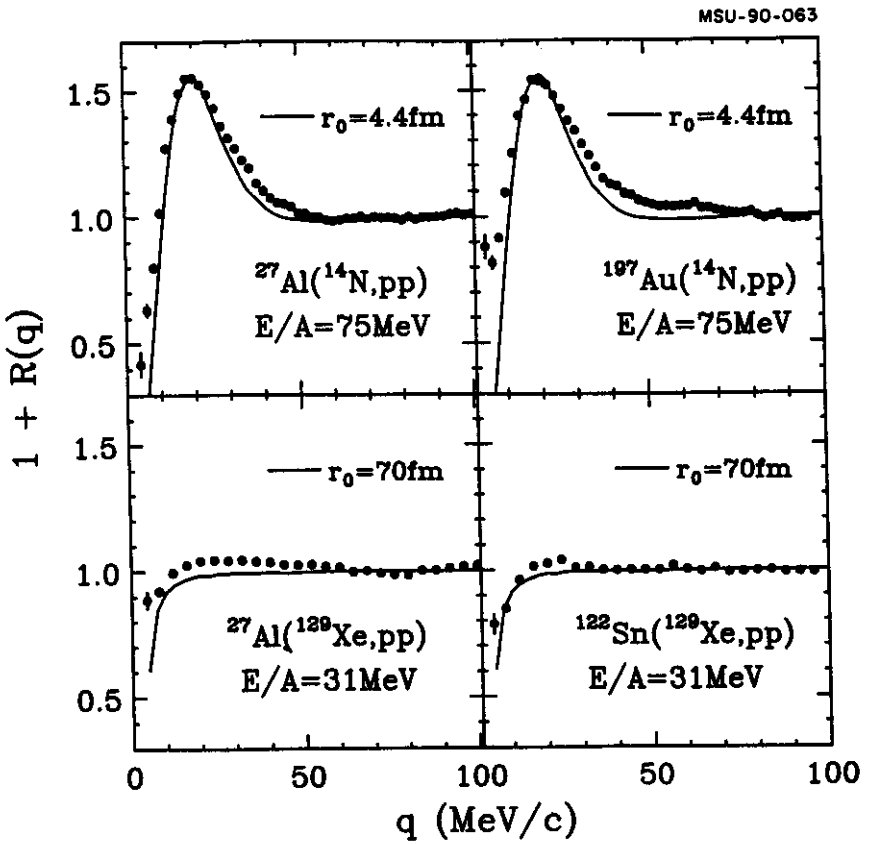

Fig. 2. Comparison of energy integrated two-proton correlation functions measured for the reactions $^{14}N+^{27}Al$ and $^{14}N+^{197}Au$ at E/A=75 MeV (top panels) and the reactions $^{129}Xe+^{27}Al$ and $^{129}Xe+^{122}Sn$ at E/A=31 MeV (bottom panels). The solid curves represent correlation functions predicted for Gaussian sources of negligible lifetime for the indicated radius parameters, r_0.

orientation, the solid lines show theoretical correlation functions predicted for Gaussian sources of negligible lifetime with the radius parameters r_0=4.4 and 70 fm for the reactions induced by ^{14}N and ^{129}Xe, respectively. These source parameters should be compared to the equivalent radius parameters for Al and Au nuclei, $r_0(Al)\approx 2.5$ fm and $r_0(Au)\approx 4.4$ fm , which are obtained from tabulated [16] rms charge radii, $\langle r^2\rangle^{1/2}$, using the approximate relation $r_0=0.82\langle r^2\rangle^{1/2}$. For the ^{14}N-induced reactions, a source radius of r_0=4.4 fm is not necessarily unreasonable. However, it is astonishing that this radius parameter exhibits no obvious dependence on the size of the target nucleus. A purely geometrical interpretation of the correlation function is,

therefore, in doubt. For the large source parameter, $r_0 \approx 70$ fm, used to describe the correlation functions measured for the ^{129}Xe induced reactions, a purely geometrical interpretation is clearly unphysical and the lifetime of the emitting system must play a major role.

6. DEPENDENCE ON TOTAL MOMENTUM

Two-proton correlation functions are known to exhibit strong dependences on the energy of the emitted particles [2-6,8] or, equivalently, on the total momentum, $\vec{P}=\vec{p}_1+\vec{p}_2$, of the coincident particle pair. Figures 3 and 4 show correlation functions for representative ranges of the total momentum, P, for the reactions $^{14}N+^{27}Al$ and $^{14}N+^{197}Au$, respectively. Consistent with previous measurements, the maximum at $q \approx 20$ MeV/c becomes more pronounced for

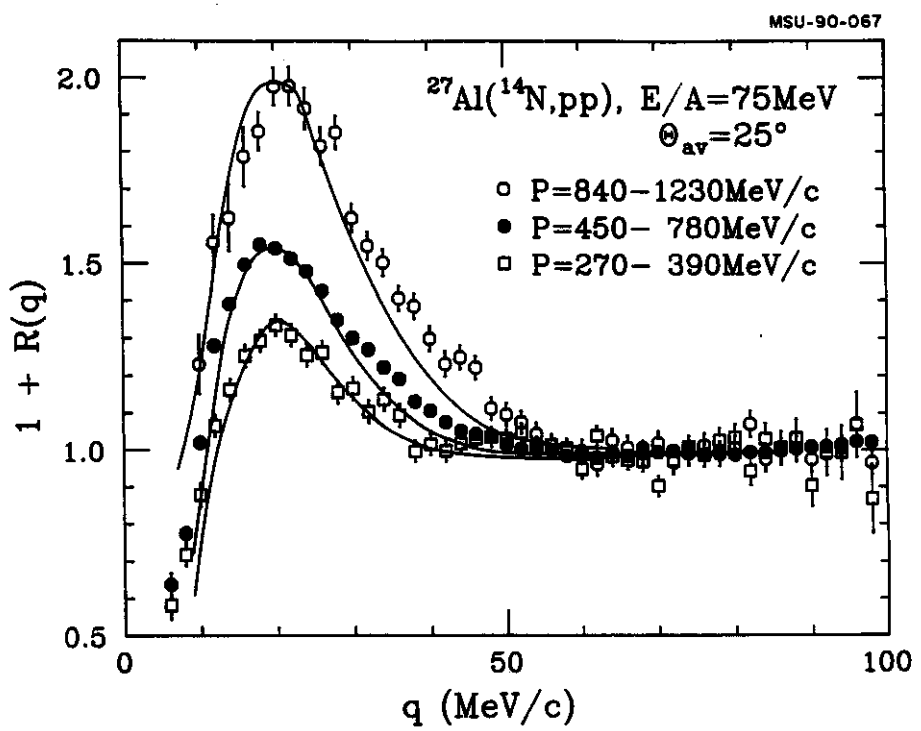

Fig. 3. Two-proton correlation functions measured for the reaction $^{14}N+^{27}Al$ at E/A=75 MeV. The gates placed on the total momenta, P, of the coincident particle pairs are indicated. The solid curves represent calculations for Gaussian sources of negligible lifetime, assuming a dependence of the radius parameter, r_0, on total momentum, P, as shown by the open points in Fig. 6 and folding in the response of the experimental apparatus.

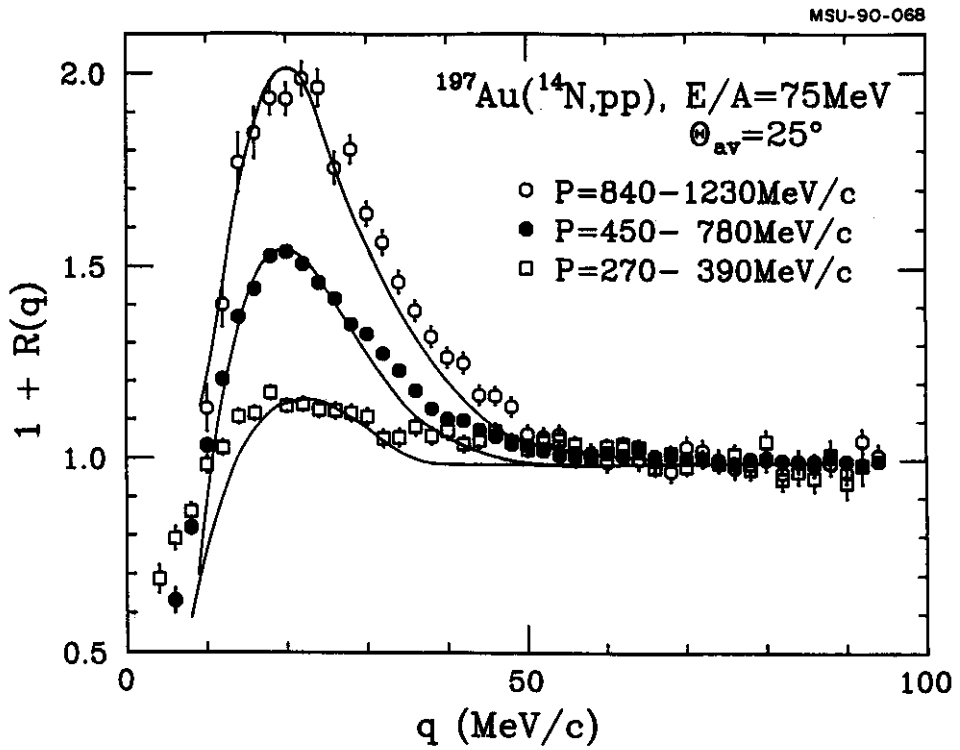

Fig. 4. Two-proton correlation functions measured for the reaction ^{14}N+^{27}Al at E/A=75 MeV. The gates placed on the total momenta, P, of the coincident particle pairs are indicated. The solid curves represent calculations for Gaussian sources of negligible lifetime, assuming a dependence of the radius parameter, r_0, on total momentum, P, as shown by the solid points in Fig. 6 and folding in the response of the experimental apparatus.

larger total momenta, i.e. for the emission of more energetic particles. For the lowest momentum gate, P=270-390 MeV/c, the correlation functions are distinctly different for the two targets. For the ^{27}Al target, a clear maximum at q≈20 MeV/c is measured. For the ^{197}Au target, on the other hand, this maximum is barely visible and the shape of the correlation function resembles that measured for evaporative processes.

Correlations measured for the ^{129}Xe-induced reactions exhibit a less dramatic dependence on the total momentum of the detected proton pair. Figure 5 shows two-proton correlation functions for two representative momentum gates, measured for the reactions ^{129}Xe+^{27}Al (upper panel) and ^{129}Xe+^{122}Sn (lower panel). The momentum gates represented by the solid and open points correspond to protons emitted

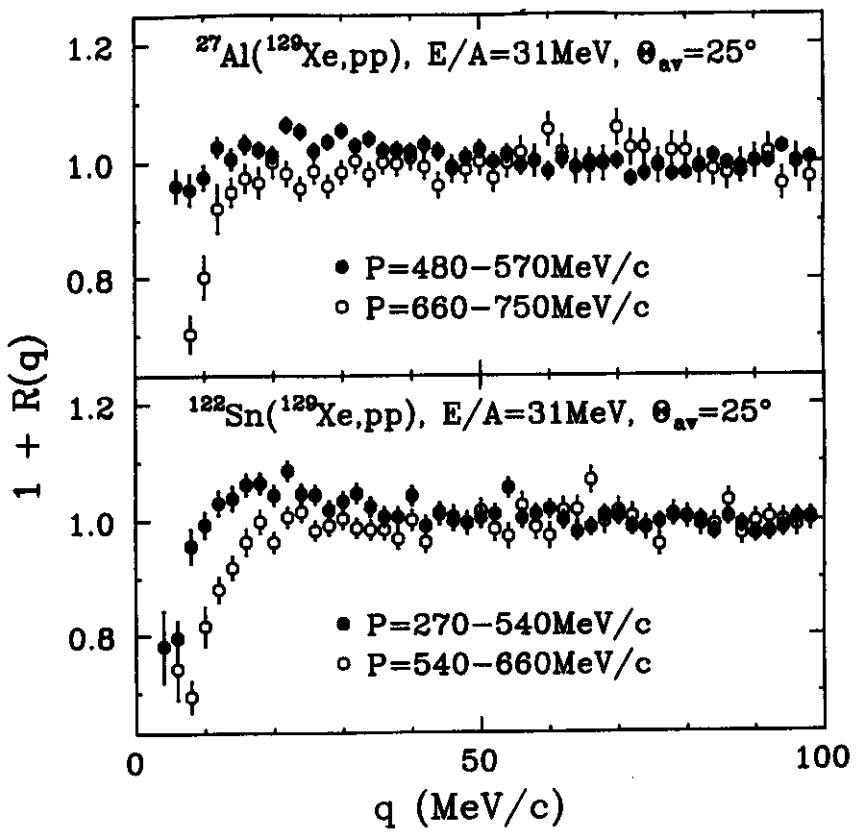

Fig. 5. Two-proton correlation functions measured for the reactions ^{129}Xe+^{27}Al and ^{129}Xe+^{122}Sn at E/A=31 MeV. The gates on the total momenta, P, of the coincident proton pairs are indicated; solid and open points represent center-of-mass energies below and above the compound nucleus Coulomb barriers.

with kinetic energies below and above the compound nucleus Coulomb barriers, respectively. As can be expected from qualitative time scale arguments, sub-barrier emission results in a reduction of the minimum at q≈0 MeV/c. At sub-barrier energies, the correlation functions are also more sensitive to attenuations and/or distortions from sequential decays of primary fragments emitted in particle unbound states [5,12] and from deflections in the Coulomb field of the heavy reaction residue. Because of these additional complications, we will refrain from a more detailed analysis of two-proton correlation functions for particles emitted with sub-barrier energies.

In order to describe the dependence of the measured two-proton correlation functions on total momentum in terms of a simple variable,

we have constructed experimental correlation functions for a number of narrow gates placed on the total momentum P. For each such correlation function we extracted the source parameters, r_0, of Gaussian sources of negligible lifetime, Eq. (5), for which the predicted correlation functions were consistent with the data. The dependence of the extracted parameters, r_0, on the total momentum of the detected particle pair is shown in Fig. 6. The error bars indicate estimated systematic errors. The solid curves in Figs. 3 and 4 show correlation functions calculated for Gaussian sources for which the radius parameter r_0 was assumed to exhibit the dependence on total momentum shown in Fig. 6. In these calculations, appropriate averages over total momentum and the calculated resolution of the hodoscope were taken into account. The overall trends of the data are well described. However, for the $^{14}N+^{197}Au$ reaction, the adopted parametrization fails to reproduce the exact shape of the minimum at q≈0 MeV/c for the low momentum gate, P=270-390 MeV/c. Here, contributions from much larger

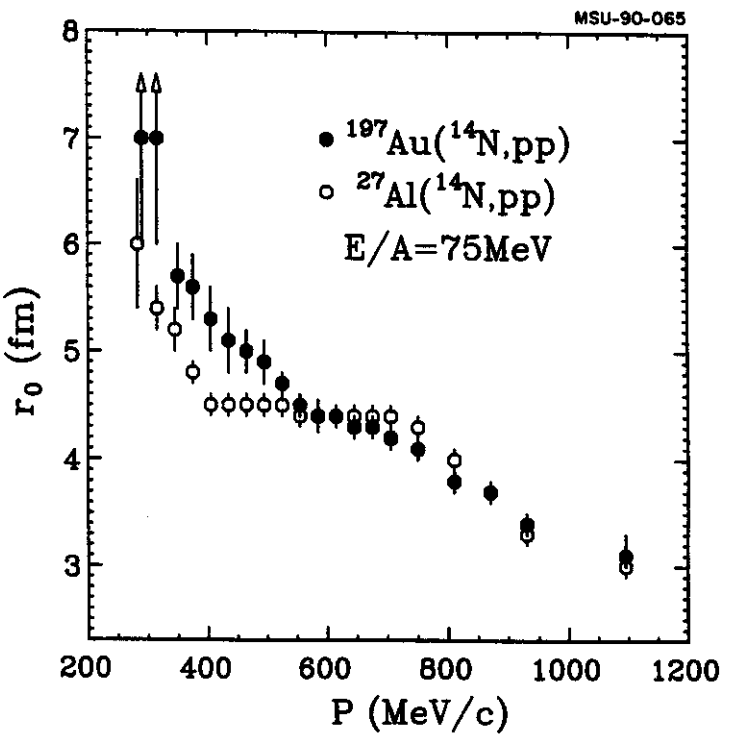

Fig. 6. Radius parameters, r_0, for Gaussian sources of negligible lifetime extracted from two-proton correlation functions gated by different total momenta, P, of the coincident particle pairs for ^{14}N induced reactions on ^{27}Al and ^{197}Au at E/A=75 MeV. The error bars indicate estimated systematic errors.

sources or, alternatively, from long lived evaporative processes would be required to fit the data. We did not attempt to improve the description by assuming a superposition of sources of different dimensions or life-times.

While the average correlation functions measured for the $^{14}N+^{27}Al$ and $^{14}N+^{197}Au$ reaction are very similar (see Fig. 2), significant differences surface when one explores the dependence on the total momentum of the proton pairs. Such more subtle differences, already apparent in the raw data shown in Figs. 3 and 4, are clearly revealed in Fig. 6. For the $^{14}N+^{197}Au$ reaction, the extracted source dimensions exhibit a nearly monotonic increase with decreasing total momentum of the detected particle pair. For the $^{14}N+^{27}Al$ reaction, on the other hand, the extracted source dimensions are rather constant over the range of $P\approx400$-750 MeV/c. The extracted source dimensions are comparable for the two targets at high total momenta, $P\gtrsim800$ MeV/c, indicating that very energetic particles are emitted by comparable processes. At low total momenta, $P\lesssim500$ MeV/c, the extracted source dimensions are considerably larger for the reactions on ^{197}Au than for the reactions on ^{27}Al, most likely indicating larger contributions from slow evaporation processes for the ^{197}Au target.

7. EVAPORATIVE EMISSION

We have used the statistical model of ref. [12] to construct Wigner functions for evaporative emission from equilibrated compound nuclei. In this model, the average particle emission is calculated from the Weisskopf formula and cooling of the compound nucleus is calculated from the average mass and energy emission rates. Sub-barrier emission is not incorporated because of the use of the sharp cut-off approximation for the inverse cross sections. For simplicity, the level density is approximated by that of an ideal Fermi gas.

In Fig. 7, results of these evaporation calculations are compared with two-proton correlation functions measured for the $^{129}Xe+^{27}Al$ and $^{129}Xe+^{122}Sn$ reactions. The curves represent calculations which were folded with the resolution of the experimental apparatus and averaged

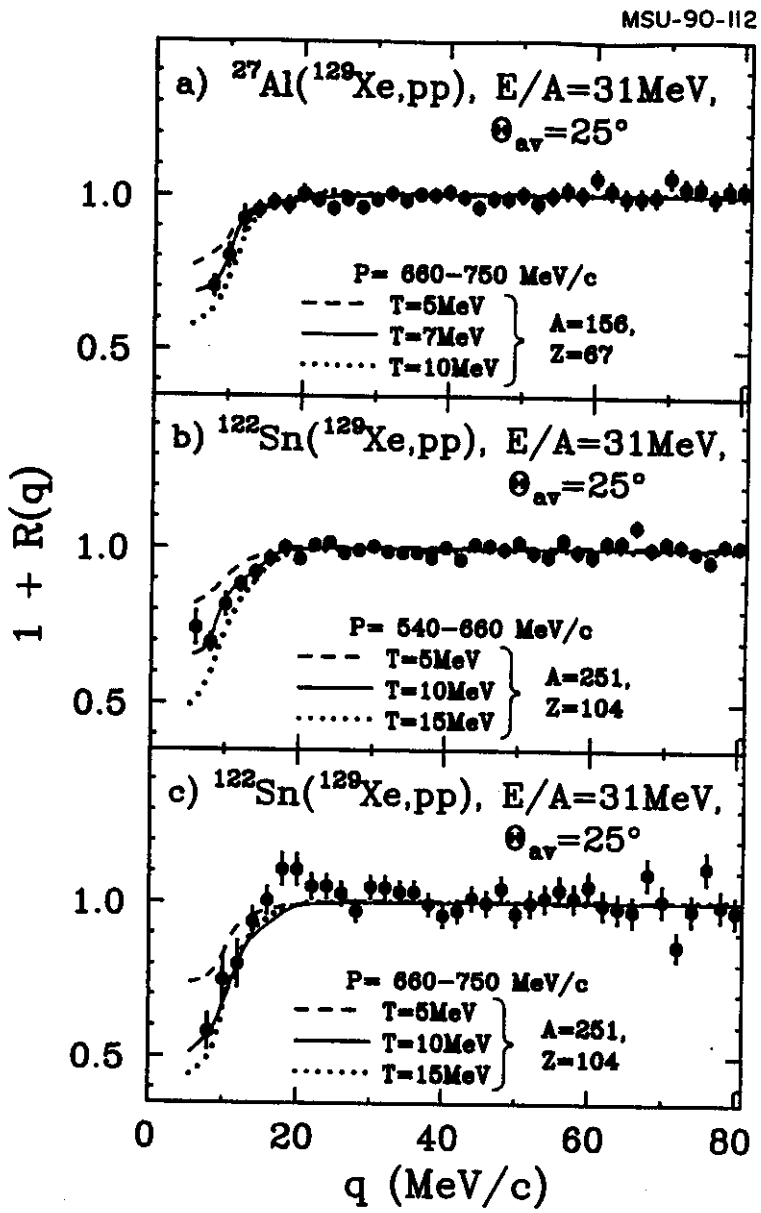

Fig. 7. Two-troton correlation functions measured for the ^{129}Xe+^{27}Al (part a) and ^{129}Xe+^{122}Sn (parts b,c) reactions at E/A=31 MeV for the indicated gates on the total momenta, P, of the proton pairs. The curves represent calculations for evaporative sources with parameters indicated on the figure.

over the appropriate momentum bins using the experimental proton yields as relative weights. The parameters used in these calculations (initial mass, A, charge, Z, and temperature, T, of the decaying nucleus) are indicated in the figure; normal nuclear density was assumed. In order to illustrate the sensitivity of the calculated emission rates to the

initial temperature of the emitting system, we used the compound nucleus values for A and Z, but treated the temperature as a free parameter. For complete fusion of ^{129}Xe+^{27}Al and ^{129}Xe+^{122}Sn, temperatures of 8.2 and 10.3 MeV, respectively, are calculated if one assumes the level density of an ideal Fermi gas of normal nuclear matter density; the more common relation, $T^2=(8\ \mathrm{MeV})E^*/A$, gives values of 5.8 and 7.3 MeV. However, the equilibrated emitting systems should have temperatures which are somewhat lower than those calculated for compound nuclei formed in complete fusion reactions [5,17-19] since some energy is carried away by preequilibrium emission. Good agreement between calculations and data is obtained for initial temperatures of about 7-10 MeV, see Fig. 7.

We have explored the dependence of the two-particle correlation function on the angle, $\Psi = \mathrm{acos}\left(\vec{P}\cdot\vec{q}/Pq\right)$, between the relative and total momentum vectors of the two-proton pair to search for clues on the source lifetime and shape [1,7,8,11]. Emission from long-lived systems produces Wigner functions elongated in the longitudinal direction [7,8]. Because of the reduced Pauli anti-correlation in this direction, the longitudinal correlation function ($\Psi\approx 0°$ or 180°) of a long-lived source may be enhanced compared to the transverse correlation function ($\Psi\approx 90°$), unless the average particle separations become so large that sensitivity to antisymmetrization effects is lost. Figure 8 shows longitudinal and transverse two-proton correlation functions measured for the ^{129}Xe+^{27}Al (top panel) and the ^{129}Xe+^{122}Sn reactions. The longitudinal correlation functions, shown by solid points, were evaluated for the gate $|\cos\Psi|\geq 0.77$ (corresponding to the angular cuts of Ψ=0°-40° or 140°-180°). The transverse correlation functions, shown by open points, were evaluated for the gate $|\cos\Psi|\leq 0.5$ (corresponding to the angular cut of Ψ=60°-120°). For improved statistical accuracy, the gates on the total momenta of the proton pairs were made wider than in Fig. 7; the values are indicated in the figure. No statistically significant difference between longitudinal and transverse correlation functions is visible. However, this result does not contradict theoretical expectations for evaporation from long-lived compound nuclei. The solid and dotted curves in Fig. 8 show longitudinal and

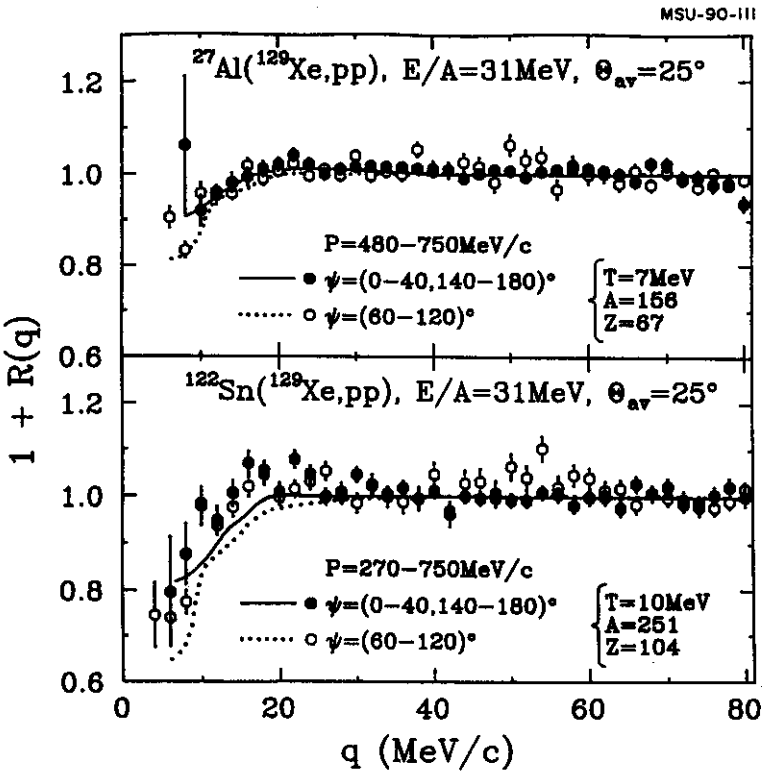

Fig. 8. Longitudinal (Ψ=0°-40° or Ψ=140°-180°) and transverse (Ψ=60°-120°) two-proton correlation functions measured for the reaction ^{129}Xe+^{27}Al (top panel) and ^{129}Xe+^{122}Sn (bottom panel) at E/A=31 MeV. The normalizations were determined from the Ψ-integrated data.

transverse correlation functions calculated for evaporative emission using the parameters indicated in the figure. The calculations were averaged over the appropriate momentum bins and folded with the resolution of the experimental apparatus. The predicted differences between transverse and longitudinal correlation functions are of the order of a few percent and, therefore, below the statistical sensitivity of the present experiment.

8. NONEQUILIBRIUM EMISSION

We have used the semiclassical Boltzmann-Uehling-Uhlenbeck (BUU) equation [20,21] to obtain Wigner functions for non-equilibrium emission processes. The BUU equation describes the temporal evolution of the one-body density under the influence of the nuclear mean field

and individual nucleon-nucleon collisions. The Pauli exclusion principle is included semiclassically by suppressing collisions into occupied regions of phase space.

In our calculations, we approximated the mean field potential by a density-dependent Skyrme-type parametrization,

$$U(\rho) = -124(\rho/\rho_0) + 70.5(\rho/\rho_0)^2. \qquad (5)$$

This parametrization is conventionally referred to as a "stiff" equation of state with nuclear compressibility, K=380 MeV. The in-medium nucleon-nucleon cross section is approximated by the energy-dependent free nucleon-nucleon cross section, parametrized from experimental data. The calculations were terminated at a time of 160 fm/c after the nuclei came into contact. Nucleons were considered as emitted when the surrounding density fell below $\rho=\rho_0/8$, where ρ_0 denotes the density of normal nuclear matter.

In Fig. 9, preliminary results of such calculations, averaged over

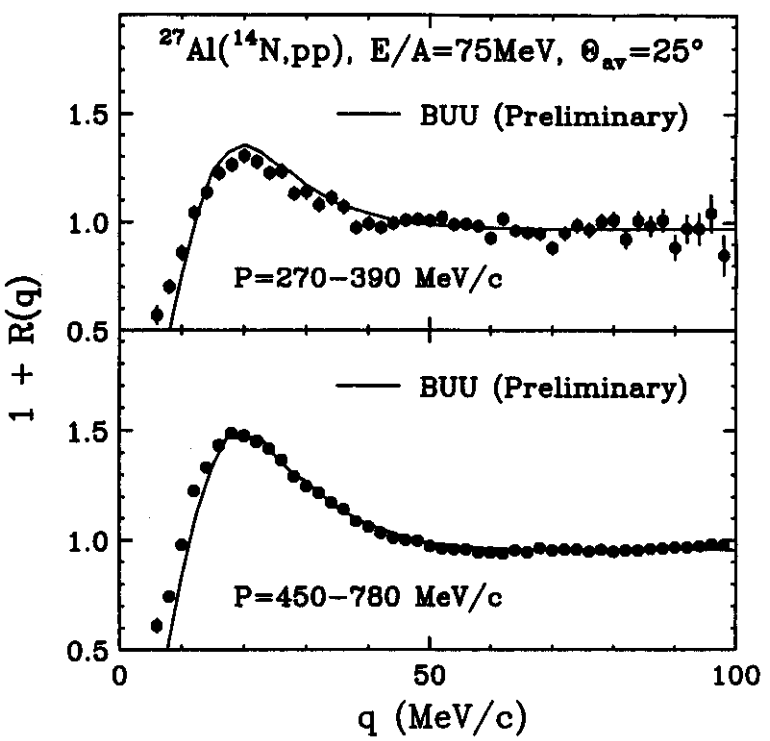

Fig. 9. Comparison of experimental and theoretical two-proton correlation functions for ^{14}N+^{27}Al collisions at E/A=75 MeV for the indicated gates on the total momenta, P, of the proton pairs. The calculations are explained in the text.

impact parameter and appropriate momentum bins, are compared to the experimental correlation functions for the $^{14}N+^{27}Al$ reaction. Because of lack of statistical accuracy, we only present calculations for the lower two momentum bins shown in Fig. 3. These preliminary results are encouraging: the calculations reproduce the overall magnitude of the measured correlation function, indicating that the overall time-scale of the collision process is correctly predicted by the BUU equation.

9. ACKNOWLEDGEMENTS

This work is based upon work supported by the National Science Foundation under Grant numbers PHY-86-11210 and PHY-89-13813 and the Department of Energy under grant number DE.FG602-88ER.40404.A000. WGL acknowledges the receipt of U.S. Presidential Young Investigator Award and NC acknowledges partial support by the FAPESP, Brazil.

10. REFERENCES

1. S.E. Koonin, Phys. Lett. 70B,43(1977).
2. W.G. Lynch et al., Phys. Rev. Lett. 51,1850(1983).
3. Z. Chen et al., Phys. Rev. C36,2297(1987).
4. Z. Chen et al., Phys. Lett. B186,280(1987).
5. J. Pochodzalla et al., Phys. Rev. C35,1695(1987).
6. J. Pochodzalla et al., Phys. Lett. B174,36(1986).
7. S. Pratt and M.B. Tsang, Phys. Rev. C36,2390(1987).
8. T.C. Awes et al., Phys. Rev. Lett. 61,2665(1988).
9. P.A. DeYoung et al., Phys. Rev. C39,128(1989).
10. J. Quebert et al., Proc. Sympos. Nucl. Dynamics and Nucl. Disassembly, Dallas, April 1989, ed. J.B. Natowitz, World Scientific, Singapore 1989, p. 337.
11. D. Ardouin et al., University of Nantes, Internal Report LPN-89-02.
12. W.A. Friedman and W.G. Lynch, Phys. Rev. C28,16(1983).
13. J. Aichelin and G. Bertsch, Phys. Rev. C31,1730(1985).
14. W. Cassing, Z. Phys. A329,471(1988).
15. W.G. Gong et al., Nucl. Instr. and Meth. A268,190(1988).
16. B.A. Brown et al., J. Phys. G10,1683(1984).
17. R. Wada et al., Phys. Rev. C39,497(1989).
18. D.X. Jiang et al, Nucl. Phys. A503,560(1989).
19. H.M. Xu et al., Phys. Rev. C40,186(1989).
20. G.F. Bertsch and S. Das Gupta, Phys. Rep. 160,L89(1988), and references given there.
21. A detailed account of the numerical details is given in W. Bauer, Michigan State University report MSUCL-699, submitted to Phys. Rev. C.